EXPERIMENTAL STUDY ON THE EFFECT OF SPRAY CONE ANGLE ON THE CHARACTERISTICS OF HORIZONTAL JET SPRAY FLAME UNDER SUB-ATMOSPHERIC PRESSURE

Kai XIE[1], Xingqi QIU[1], Yunjing CUI[2*], Jianxin WANG[3]

[1] College of Chemical Engineering, China University of Petroleum (East China), China

[*2] College of Electromechanical Engineering, China University of Petroleum (East China), China

[3] Yunnan Aerospace Industry Co. Ltd, Kunming, China

[*] Corresponding author; E-mail: cuiyj@upc.edu.cn

The burning state of a plateau environment is attracting more and more attention. In this paper, in order to have a deeper scientific understanding of diesel spray combustion and the characteristics of a flame under different spray cone angles in a plateau environment, experiments were carried out in a low-pressure chamber. The flame morphology was recorded by a high-speed video instrument, and the temperature change was recorded by a thermal imager and thermocouples. MATLAB programming was used to process the video image of the flame, and the probability of its binarization was calculated. The results indicate that the flame becomes longer and wider under different pressures with the same spray angle. The variation is more pronounced at a smaller spray taper angle. The flame uplifted height characteristic is mainly negatively related to the atmospheric pressure. According to the normalized flame temperature and the dimensionless horizontal projection, the length can be divided into three regions. In the region of buoyancy flame, the dimensionless temperature varies with sub-atmospheric pressure more than with normal pressure. In addition, under different spray cone angle conditions, the law of variation in the normalized flame temperature under sub-atmospheric pressure is exactly opposite to that under normal pressure. This study is of great significance to the scientific research on flames in a low-pressure environment, and the design of different fuel nozzles for application in a plateau environment.

Key words*: spray cone angle, spray flame, horizontal uplifted height, flame temperature, sub-atmospheric pressure*

1. Introduction

Pressure-atomizing nozzles are widely used in various industrial processes, including in oil burners [1]. The spray cone angle is the angle between the two tangents from the outlet of the nozzle to the spray-moment outsourcing line. The spray cone angle is a core parameter of a pressure-atomizing nozzle. The atomizing distribution of a droplet is determined by the spray cone angle [2]. Previous scholars have conducted in-depth theoretical and experimental studies on this issue, and found that the spray cone angle has a decisive influence on the spray liquid's flow rates [3], the droplet

size distribution [4], the final flame shape [5], and temperature characteristics [6-9]. It is generally accepted that, with an increase in the spray cone angle at the same flow rate, the spray penetration distance decreases and the flame becomes wider and shorter. Igor et al. [10] carried out an experimental study on the nozzles in a fuel oil boiler and found that a larger spray cone angle can enhance the spatial dispersion of droplets at the burner's outlet region. Consequently, the flames become wider and shorter. Sidey et al. [11] investigated the swirling spray flame stability of a 60° hollow cone angle employing a C_7H_{16}–CH_4 dual fuel. Verdier [12] investigated the local flame structure with a simplex Danfoss nozzle (1.35 kg/h, 80° hollow cone) by the OH-PLIF images method. However, these experiments were conducted under normal atmospheric pressure. Whether the flame's morphology and the temperature characteristics of a liquid spray flame under sub-atmospheric pressure are consistent with those under atmospheric pressure has not been fully reported.

At present, the burning state of a plateau environment is being paid more and more attention. Fuel spray flames may become longer or shorter under sub-atmospheric pressure [13]. Some experimental studies have been carried out on various flames in a low-pressure environment, and, generally, similar laws have been found. Most investigations are concerned with a laminar flame [14] and gas combustion. Kim et al. [15] carried out an experimental study on a laminar acetylene diffusion flame under 0.01~0.10 MPa. Hu, Li, and Zhang et al. conducted an experimental investigation on acetylene [16,17] and propane [18] diffusion flames in 0.64 atm and 1 atm environments, respectively. Wang et al. [19,20] investigated the lift-off height of a turbulent propane diffusion flame in a vertical jet and the flame morphology under the influence of a cross-flow wind in a low-pressure chamber. They found that, under an atmospheric pressure of 0.64 atm, both acetylene and propane flames are stretched. Furthermore, the lift-off height of the flame is exponentially related to the atmospheric pressure. For liquid combustion, the systematic laboratory research can be traced to Wieser's experiments. Wieser et al. [21] conducted n-heptane combustion tests at an altitude of 400–3000 m (71–97 kpa) in a European standard EN54 test chamber. Similar further experimental studies of n-heptane combustion at low pressure have been performed [22-24]. In addition, Liu et al. [25] compared the temperature characteristics of three fuels (ethanol, n-heptane, and jet-A) at an altitude of 3650 m. Their studies found that the flame center line temperature at a high altitude was lower than that at a lower altitude. These studies are also mostly related to oil basin fires and pool fires, and the flame's forms in these studies are all vertical. For a liquid spray flame, there has been less investigation at a low pressure. For a vertically burning flame, the buoyancy usually produces an upward thrust at the terminal flame region. Similarly, for a horizontal jet flame, unless the jet's momentum is particularly large, uplifted height characteristics will also occur in the terminal flame region. In fact, at a low atmospheric pressure, the reduced air density will result in a different air entrainment at the terminal flame region. Therefore, the buoyancy-driven behavior under sub-atmospheric pressure must be different from that in an atmospheric environment. Even for a liquid spray horizontal jet flame at low pressure, almost no studies are available. However, at present, there is an urgent need for research on its application in a plateau environment.

In this paper, a study was conducted in a low-pressure chamber. Solid mechanical pressure-atomizing nozzles with different spray cone angles (45°, 60°, and 80°, respectively) were used in the experimental study in the low-pressure chamber in an atmospheric pressure range of 0.05–0.10 MPa (the corresponding altitude is about 5500~0 m). We will focus on the changes in the flame

morphology and the temperature characteristics under different spray cone angle conditions in a sub-atmospheric pressure environment.

2. Experiment and method

2.1 Experimental setup

As local experiments at different altitudes are difficult to achieve, a sealed low-pressure chamber is applied in this study. The dimensions of this low-pressure chamber are 3 m (length) x 2.5 m (height) x 3 m (width). Of course, in order to assess the reliability of the experiment, we conducted in-chamber and out-chamber comparison experiments under local pressure (Kunming, China, 0.08 MPa), and the flame's morphology and temperature were basically consistent. Figure 1 shows a schematic diagram of the experimental device. A RIELLO G40 diesel burner was used in the experiment. The test chamber's temperature was controlled at 20±2℃. The pressure range that was provided by the test chamber was 0.045~0.10 MPa with an accuracy of ±100 Pa. A continuous supply of fresh air can be realized, and the new air volume can be adjusted continuously from 0 to 200 cubic meters per hour, which fully satisfied the experiment's air supply demand. A Danfoss solid pressure-atomizing nozzle was applied in the experiment, and the injection pressure was kept constant at 0.12 MPa. The fuel was 0# diesel. The burning power was also kept constant at 36 kW. In order to monitor the combustion situation, a TESTO gas analyzer was applied in the test. In this study, the flue gas analyzer was only used to ensure that the combustion was well-monitored, and was not used to analyze the pollutant. Similarly, as the burner remained unchanged, the swirl intensity that the swirl stabilizer generated for the spray combustion was not considered in this study.

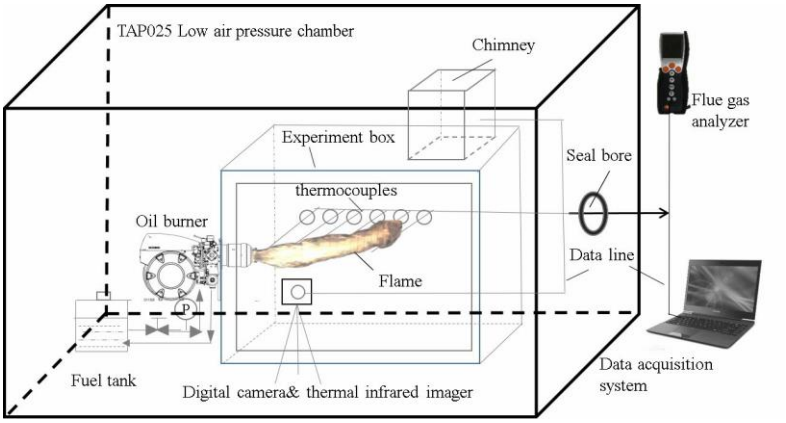

Figure 1. The diagram of the experimental combustion facility in the low-pressure test chamber

During the experiment, the condition of a steady flame and the fuel and air intake quantities were kept unchanged, and different nozzles could be replaced, respectively. In the experiment, the range of oscillation of the oscillating spray angles was affected by the oil pressure, the air inlet volume, the cyclone intensity, etc. In the research process, due to the other conditions remaining unchanged, only the different nominal spray angles could be investigated. Figure 2 shows a diagram of the spray cone angle of the pressure-atomizing nozzle that was used in this study. The experimental scheme is shown in tab. 1

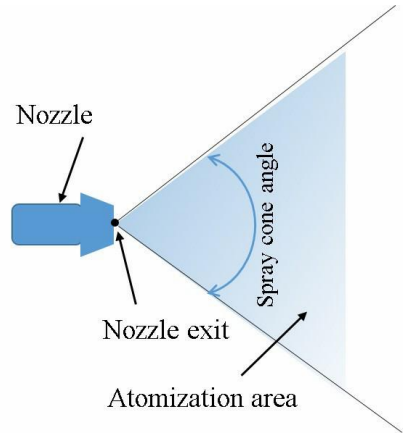

Figure 2. The spray cone angle diagram

Table 1. Experimental scheme table

Case No.	Atmospheric pressure [MPa]	Spray cone angles [degree]	Quantity of fuel [kg/s]
1	0.05	45	3
2	0.075	45	3
3	0.10	45	3
4	0.05	60	3
5	0.075	60	3
6	0.10	60	3
7	0.05	80	3
8	0.075	80	3
9	0.10	80	3

Flame morphology and temperature are two main characteristics of combustion [26,27]. In the low-pressure test chamber, the two features were measured precisely, and a data analysis was subsequently carried out. When testing the temperature of the flame trajectory, a number of holes were opened in the back of the test box to fix and adjust the position of the thermocouple, and a thermal imager was used to assist in testing the temperature of the flame, which was calibrated before the test. The test equipment and the data recording system were inside and outside of the cabin, respectively, which included the following elements:

- thermal imager, ThermaCAMTMS65, 50 FPS, sensitivity: ±2℃
- videocassette recorder, SONY HDR - CX360E, 50 FPS, size of 1920 pixels x 1080 pixels
- thermocouples, K type, diameter 0.5mm, sensitivity:±1.5℃
- A/D converter, I—7018 modules, the sampling rate is 10 times per second, accuracy±0.1%
- flue gas analyzer, TESTO 330, sensitivity: O_2 Vol.: ±0.2 %, CO: ±1.0 ppm

2.2 Flame image processing

Flame configuration parameter is one of the important parameters of flame characteristics [28]. The direct measurement of a flame dimensions in an image is still a major issue in many studies [29]. The flame height fluctuates periodically due to the instability of the flame and the surrounding air

boundary layer. Such a direct mark measurement has obvious accuracy defects. Therefore, we need to consider the probability statistics of the occurrence of brightness in the intermittent flame region within a time series. The original video of the flame that was taken in the low-pressure cabin needs to be processed before the probabilistic statistical calculation of the flame image time series can be performed. The processing process mainly includes video interception, gray processing of the image, optimal threshold selection, image segmentation, and probability statistics of the brightness.

As the radiation intensity of the flame in each experiment is inconsistent, the brightness of the flame in the video will be different, and the optimal threshold for each experiment's treatment will be different. If the threshold is too large, a portion of the flame's effective area will be lost, and if the threshold is too small, there will be a lot of background noise in the image. Because the collection of the video of the flame in this study is carried out in a test box with low brightness, the high brightness of the flame forms a strong contrast with the dark environment around it. In this study, the bimodal method is used to find the optimal threshold value. The optimal threshold value of the flame image in this study is determined according to the gray level of two parts' mutation in the average time sequence of the gray image, as shown in the gray histogram in fig.3. As can be seen from the histogram, there is a distinct wave trough between the two peaks, and the optimal threshold is the gray value that corresponds to the wave trough.

The average grayed flame images were segmented according to the optimal threshold value. The segmented image can be divided into two parts. One part is the highlighted area that we need to count, and the other part can be regarded as the interference area. The probability of the flame's effective partial brightness was calculated. In the image processing process used in this study, 12 s was selected for the stable combustion video in each case. A total of 300 frames of images were processed, and, eventually, 300 frames of binary flame images were obtained. Taking the experiment's Case 1 as an example, the main process for flame image processing is shown in fig.4.

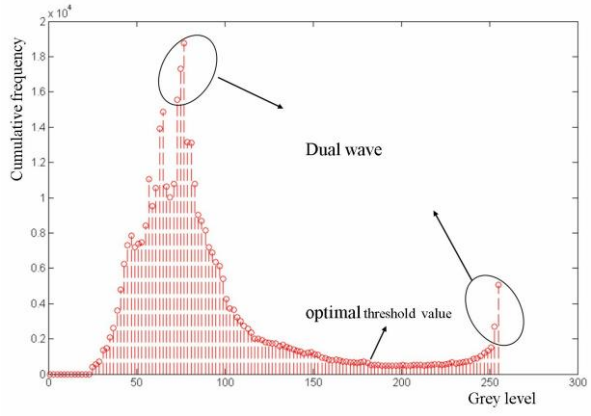

Figure 3. A histogram of a mean gray flame image

Statistics were obtained on the number of white spots in each position, and the flame's average probability distribution contour was finally obtained, as shown in fig.5. The position where the flame occurrence probability is 50% is defined as the flame terminal. In the contour, its horizontal average flame length *L*, maximum width *W*, horizontal uplifted height *H*, and characteristic slope *k* are defined and described.

The size of the flame horizontal uplifted height, etc. were determined based on the pixel size in the image and the actual scale. In addition, the diameter of the burning cylinder is 80 mm, and the size of the internal test box is 800(*L*)*600(*H*) mm. Based on this, the image's scale was determined, and the flame actual structural data were finally obtained.

Figure 4. The main flame image processing process; (a) original flame (b) gray flame, and (c) binary flame

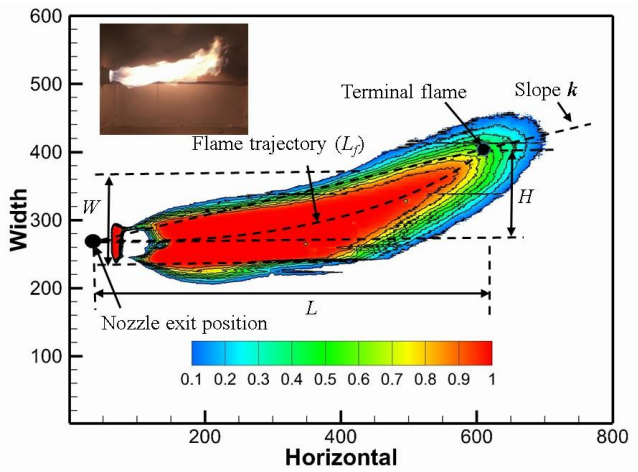

Figure 5. The definition of the parameters in a flame probability distribution contour

3. Results and discussion

The spray cone angle reflects the range of droplet distribution after leaving the nozzle. It can cause changes in a flame morphology and temperature distribution. In the following sections, we analyze the laws of variation in a flame morphology and temperature characteristics under sub-atmospheric pressure. The morphology of a flame includes the length of the horizontal projection of the flame, the maximum flame width and its position, the uplifted height of the flame terminal, and the slope of the uplifted height characteristic. With respect to the flame temperature, the temperature distribution of the flame trajectory is discussed, and the dimensionless distribution is analyzed.

3.1 Flame morphology

After the data were processed (please refer to Section 2.2 for details), the average probability of the flame morphology for the experimental Cases 1 to 9 was obtained and is shown in fig. 6. It is obvious that the flame becomes more elongated with a decrease in the atmospheric pressure and spray cone angle. Additionally, the uplifted height of the terminal flame is also increased. When the

atmospheric pressure is constant, the flame becomes shorter and thicker as the spray cone angle increases. This variation is even more pronounced as the atmospheric pressure decreases.

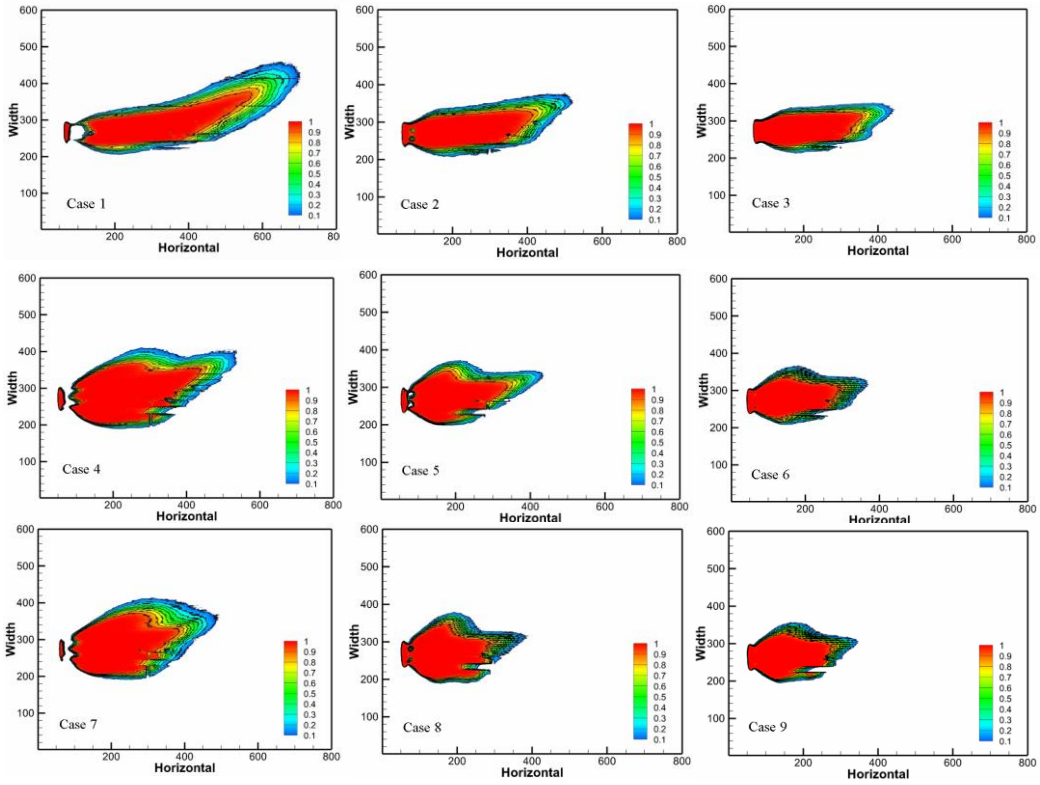

Figure 6. The flame probability distribution contour of experimental Cases 1 to 9

Figure 7 shows the specific change values of the horizontal flame projection length with atmospheric pressure at different spray cone angles. With a smaller spray cone angle, the extent of the flame's elongation becomes larger as the ambient pressure decreases. Compared to 0.05 MPa and 0.10 MPa atmospheric pressure, when the spray cone angles were 45°, 60°, and 80°, the horizontal flame projection length increased by 67%, 47%, and 37%, respectively. In addition, when the atmospheric pressure was 0.10 MPa, and the spray cone angle ranged from 45° to 80°, the flame length was shortened by 20%. This law of change is consistent with the law of change for a propane horizontal jet

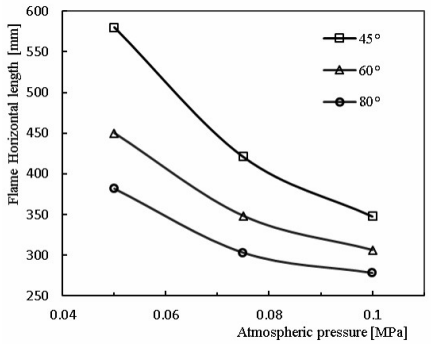

Figure 7. Horizontal flame projection length

at nozzle width in the literature [30]. However, when the atmospheric pressure was 0.05MPa, the flame length was shortened by almost 35%. The change in the flame length is closely related to the atmospheric pressure. As the air density becomes smaller under a lower pressure, the pressure difference between the front and the back of the fuel oil increases, and the flame becomes longer. As the spray angle increases, the force of the droplet that diffuses to both sides increases, and the forward momentum decreases, resulting in a shorter flame.

Figure 8 depicts the data on the flame's maximum width and position change. In general, the value of the maximum flame width increases as the atmospheric pressure decreases. However, when the spray cone angle is 45°, the widened range of the maximum flame width is slightly smaller. At the same atmospheric pressures, the maximum flame width increases roughly in a natural logarithm relation ($W \sim ln(\alpha)$) as the spray cone angle increases. In practical engineering, it is not enough to obtain a wider flame simply by increasing the spray cone angle of the burner. The position of the widest flame corresponding to the horizontal direction is mainly related to the atmospheric pressure. At sub-atmospheric pressure, the position of the maximum flame width is also shifted towards the flame front as the flame length increases. At the spray cone angles of 60° and 80°, and the atmospheric pressures of 0.075 MPa and 0.10 MPa, the location of the maximum flame width does not change along with a change in the spray cone angle. However, this situation changes with a lower atmospheric pressure and a smaller spray cone angle. As the atmospheric pressure decreases and the spray angle decreases, the position of the maximum flame width will be significantly away from the nozzle's exit. At the spray cone angle of 45°, and when the atmospheric pressure is as low as 0.05 MPa, the location of the maximum flame width shifts towards the flame front by 267% when compared with the atmospheric environment.

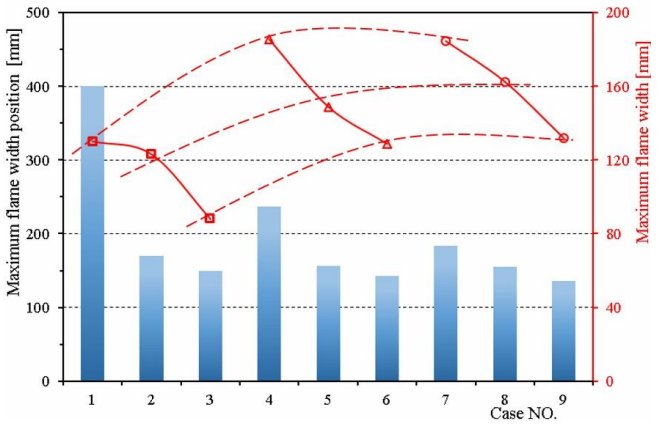

Figure 8. Maximum flame width and position

For a horizontal jet flame, the terminal flame will be uplifted in height due to the influence of air buoyancy. Figure 9 shows the uplifted height and slope of the flame uplifted height characteristic from the experimental Cases 1 to 9. Obviously, the slope k is not related to the spray cone angle, but only negatively related to atmospheric pressure. At 0.05 MPa, the slope of the flame uplifted height was about 0.205, which is 41% higher than at atmospheric pressure. Correspondingly, the law of variation for the flame uplifted height H is similar to that for a horizontal flame projection length L. Under the condition of low pressure, a decrease in atmospheric pressure has a significant effect on the flame uplifted height. Compared to 0.05 MPa and 0.10 MPa atmospheric pressure, when the spray cone angles were 45°, 60°, and 80°, the flame uplifted height increased by 133%, 102%, and 95%,

respectively. In addition, when the atmospheric pressure was 0.10 MPa, and the spray cone angle ranged from 45° to 80°, the flame uplifted height was shortened by 23%. However, when the atmospheric pressure was 0.05 MPa, the flame uplifted height was shortened by almost 36%. In fact, for a horizontal jet of flame under sub-atmospheric pressure, the phenomenon of the horizontal flame uplifted height of the flame is more significant. This is mainly because the air entrainment at the terminal flame position is more obvious at a lower pressure. In contrast, the spray angle has little effect on the flame uplifted height characteristics because the spray angle affects the overall length of the flame, so it seems that the flame's uplifted height is also affected by it. However, in fact, the decreasing or increasing length only affects the uplifted height of the flame, but does not affect the slope k of the flame uplifted height characteristics.

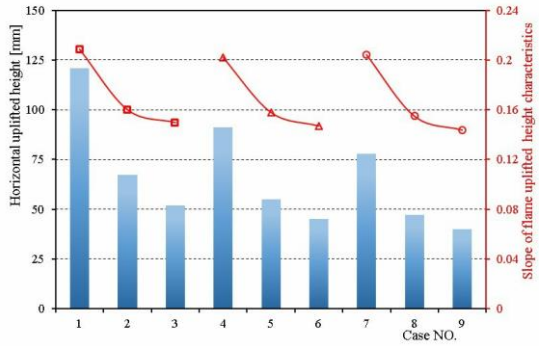

Figure 9. The flame uplifted height characteristics

3.3 Flame temperature characteristics

Flame temperature is one of the most important properties of the flame, which represents the heat released by combustion and also affects pollutant emissions. The flame temperature in this section refers to the temperature distribution along the flame's trajectory axial from the nozzle's orifice to the terminal flame. The flame temperature curves at different spray cone angles under 0.05 MPa, 0.075 MPa, and 0.10 MPa atmospheric pressure were obtained by calibrating the measured data from the thermocouples and the thermal imager, and are shown in figs. 10, 11, and 12, respectively.

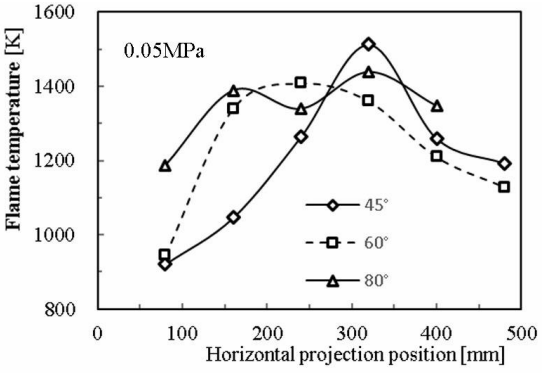

Figure 10. The temperature distribution of the flame trajectory at 0.05 MPa

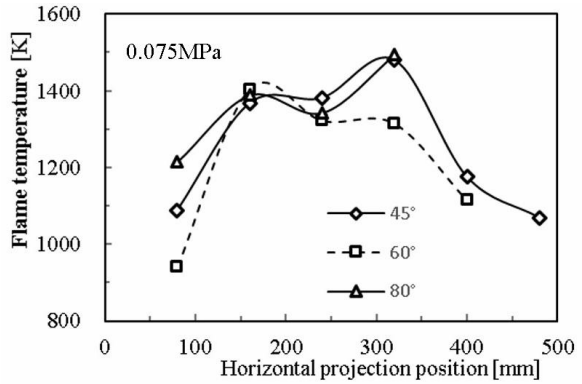

Figure 11. The temperature distribution of the flame trajectory at 0.075 MPa

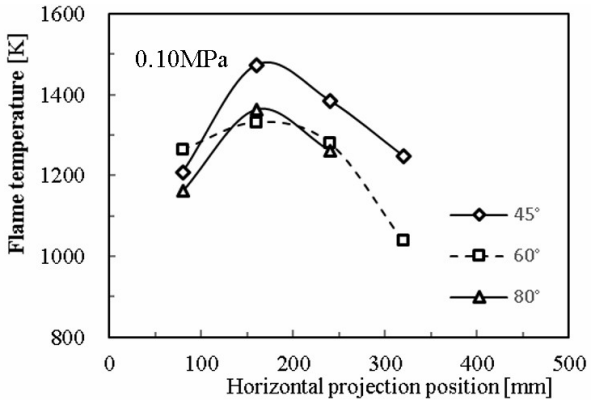

Figure 12. The temperature distribution of the flame trajectory at 0.10 MPa

In general, no matter what the ambient pressure is, at the initial stage of the flame, the flame with a larger spray cone angle has a higher combustion temperature. However, the smaller the spray cone angle, the higher the maximum temperature of the flame. The maximum temperature can reach above 1500 K. When the spray cone angles are 60° and 80°, the maximum temperature is only about 1400 K. In the buoyant flame region at the end of the flame, the flame temperature increases slightly as the spray angle decreases. As the flame becomes longer at a lower pressure, the high-temperature zone of the flame clearly moves towards the flame's front at 0.05 MPa atmospheric pressure, and the area of the cryogenic flame becomes larger.

Because the experiment was carried out under different atmospheric pressures, the change in air density needs to be considered. So, the temperature distribution of the flame trajectory axial was processed and analyzed with the dimensionless method. The characteristic axial length is expressed by $\frac{X - X_0}{D}$, where X refers to the virtual origin to normalize the difference induced by the flame ource scale [16], since the nozzle's flow rate in this study is constant and its diameter remains unchanged, and X_0 refers to the exit of the nozzle. The characteristic temperature is expressed by $\frac{T - T_0}{T_0}$, where T_0 refers to the ambient temperature. By introducing the dimensionless power Q^* [31], the flame's

trajectory axial temperature data are normalized and rendered dimensionless, as represented by the formula (1).

$$\frac{(T-T_0)}{T_0} = k\left[\frac{(X-X_0)/D}{Q^{*2/5}}\right]^{\eta} \tag{1}$$

The dimensionless flame temperature distribution with different spray cone angles and different atmospheric pressures was finally obtained as shown in fig. 13. According to the temperature distribution and flame configuration, the horizontal jet spray flame is roughly divided into three areas, including the recirculation region, the continuous flame region, and the buoyancy plume flame region. It is well-known that a spray flame needs to be stabilized, and a recirculation region will form above the flame holder. In the range of experimental conditions in this study, the temperature in the recirculation region decreases as the environmental pressure decreases; however, the temperature increases as the spray cone angle increases. This is mainly because, as the atmospheric pressure decreases, the mixing effect in the initial mixing stage of the oil mist is worse than that under normal pressure, resulting in a temperature drop. However, if the spray cone angle is increased, the droplets in this region will be more dispersed, the contact surface of the droplets and air will be increased, and the initial mixing stage can be carried out well in a sub-atmospheric pressure environment.

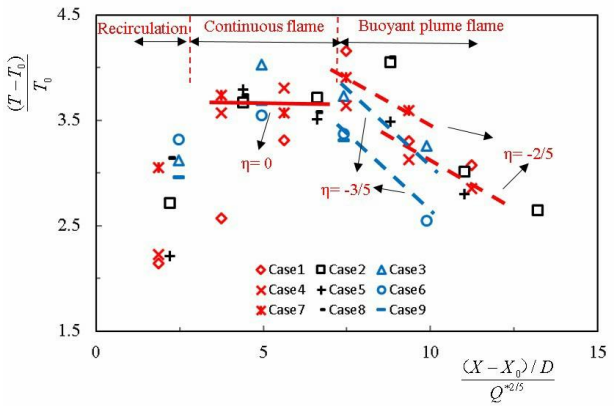

Figure 13. The correlation of dimensionless trajectory axial temperature profiles for a horizontal spray flame globally at different atmospheric pressures

In the continuous flame region, the dimensionless temperature and dimensionless horizontal projection length are parallel to the X-axis. In this case, the value of η is 0. In this region, the dimensionless temperature has little relation to the atmospheric pressure. However, generally speaking, the dimensionless temperature increases as the spray cone angle decreases.

It can be known from the analysis in the last section that the flame uplifted height characteristics are closely related to the atmospheric pressure. Similarly, the buoyancy plume flame region is greatly affected by the atmospheric pressure. We mainly compare the dimensionless temperature characteristics of the buoyancy plume flame region under a sub-atmospheric pressure. At 0.05 MPa, the dimensionless temperature value was larger than 0.10 MPa, and the plume area was longer. The corresponding values of η were -2/5 and -3/5, respectively. This indicates that, under a lower atmospheric pressure, the entrainment capacity under low-density air increases, which leads to the more obvious buoyancy-driving characteristics at the buoyancy plume flame region of the horizontal

jet spray flame. As far as the spray angle is concerned, the law of opposite variation can be found in the cases of normal atmospheric pressure and sub-atmospheric pressure. Under normal pressure, the smaller the spray cone angle is, the larger the value of k is; however, under 0.05 MPa pressure, the value of k decreases. Based on the spray characteristics of the different spray cone angles and the changes in the flame morphology under sub-atmospheric pressure, it can be known that a small spray cone angle with a higher uplifted height and a more concentrated droplet distribution leads to an inability to obtain a higher combustion temperature in the buoyancy flame area under sub-atmospheric pressure.

4. Conclusions

This article investigated the effect of spray cone angles (45°, 60°, and 80°) on the characteristics of a horizontal jet spray flame under different atmospheric pressures (0.05–0.10 MPa) by an experimental method. This mainly includes the flame morphology and the temperature distribution of the flame trajectory. The main conclusions include:

(1) With a decrease in atmospheric pressure, the length of the horizontal jet spray flame increases. The smaller the spray cone angle, the larger the increase in the flame length. The value of the maximum flame width increases as the atmospheric pressure decreases. The position of the maximum flame width is also shifted towards the flame front as the flame length increases. The slope of the flame uplifted height characteristic is affected by the air buoyancy at the terminal flame region, which is negatively correlated with atmospheric pressure.

(2) Under the same atmospheric pressure, the flame length becomes shorter as the spray cone angle increases. The maximum flame width is proportional to the natural logarithm of the spray taper angle. The position of the maximum flame width is also far away from the nozzle's outlet as the spray cone angle decreases; however, the influence force is less than that of atmospheric pressure. An increase in the spray cone angle can effectively reduce the uplifted height of the flame. Since the uplifted height varies with the length of the flame, it has no effect on the overall slope of the flame uplifted height characteristic.

(3) The dimensionless three-region theory (the recirculation region, the continuous flame region, and the buoyancy plume flame region) for horizontal jet spray flames can well-describe the temperature characteristic distribution of a flame trajectory under sub-atmospheric pressure. In the continuous flame region, the normalized temperature at low pressure is similar to that at atmospheric pressure; however, it is higher in the buoyancy plume region than at normal atmospheric pressure. The corresponding values of η were -2/5 and -3/5, respectively. The dimensionless temperature decreases as the spray cone angle increases under normal atmospheric pressure. However, in a sub-atmospheric pressure environment, the result is exactly the opposite.

Acknowledgment

This research was funded by the National Key R&D Program of China under Grant No. 2017YFC0806303.

Nomenclature

D – nozzle diameter, [mm]
k – the slope of the flame uplifted height characteristics
H – horizontal uplifted height
L – horizontal projected length, [mm]
Lf – flame trajectory length, [mm]
P – atmospheric pressure, [MPa]
Q – heat release rate, [kW]
Q^* – dimensionless heat release rate
T_0 – ambient temperature, [K]
T – flame temperature, [K]
ΔT – flame temperature rise, [K]
W – maximum flame width, [mm]
X_0 – virtual origin
X – horizontal length above the nozzle, [mm]

Greek symbols

α – spray cone angle
k – dimensionless coefficient
η – exponential constant

Subscript

0 – ambient
f – flame trajectory

References

[1] Lefebvre, A. H., McDonell V. G., *Atomization and Sprays*, CRC press, Boca Raton, USA, 2017.

[2] Dikshit, S. B., *et al*., Factors Affecting Spray Cone Angle of Pressure Swirl Atomizer for Gas Turbine Combustion Chamber: Theoretical and Experimental Analysis, *Indian Journal of Science and Technology, 11* (2018) , 8, pp. 1-4.

[3] Guo, Y., *et al.*, Experimental Study of Inclination on Non-Boiling Regime Spray Cooling, *Proceedings*, ASME 2008 International Mechanical Engineering Congress and Exposition, Boston, Massachusetts, USA, 2008, Jan., pp. 713-721.

[4] Yang, S. I., *et al.*, Spray Combustion Characteristics of Kerosene/Bio-Oil Part I: Experimental Study, *Energy, 119* (2017), Jan., pp. 26-36.

[5] Jones, W. P., *et al.*, An Investigation of a Turbulent Spray Flame Using Large Eddy Simulation with a Stochastic Breakup Model, *Combustion and Flame, 186* (2017), Dec., pp. 277-298.

[6] Datta, A., Som, S. K., Numerical Prediction af Air Core Diameter, Coefficient of Discharge and Spray Cone Angle of a Swirl Spray Pressure Nozzle, *International journal of heat and fluid flow, 21* (2000), 4, pp. 412-419.

[7] Huang, Y., *et al.*, Effect of Liquid Viscosity and Swirl Chamber Length on the Air Core And Spray Cone Angle From Pressure-Swirl Atomizers, *Proceedings*, In Energy and Mechanical Engineering:

Proceedings of 2015 International Conference on Energy and Mechanical Engineering, Hong Kong, China, 2015, pp. 642-650.

[8] Vengatesh, P., *et al.*, Spray Characteristics of Diesel Fuel Using Numerical Simulation, *International Research Journal of Engineering and Technology, 5* (2018), 4, pp. 1074-1077.

[9] Sharma, S., *et al.*, On the Effect of Spray Parameters on CO and NOx Emissions in a Liquid Fuel Fired Flameless Combustor, *Fuel, 199* (2017), Jul., pp. 229-238.

[10]Bonefačić I., *et al.*, Improvement of Fuel Oil Spray Combustion Inside a 7 MW Industrial Furnace: A Numerical Study, *Applied Thermal Engineering, 110* (2017), Jan., pp. 795-804.

[11] Sidey, J. A., Mastorakos E., Stabilisation of Swirling Dual-Fuel Flames, *Experimental Thermal and Fluid Science, 95* (2018), Jul., pp. 65-72.

[12] Verdier, A., *et al.*, Experimental Study of Local Flame Structures and Fuel Droplet Properties of a Spray Jet Flame, *Proceedings of the Combustion Institute, 36* (2017), 2, pp. 2595-2602.

[13] Xie, K., *et al.*, Experimental Study on Flame Morphology of Horizontal Jet Spray Combustion in Low Pressure Environment (in Chinese). *Industrial Heating, 47* (2018), 3, pp. 8-12.

[14] Zhong B. J., *et al.*, The Pressure Dependence of Laminar Flame Speed of 2-Methyl-2-Butene/Air Flames in the 0.1–1.0 Mpa Range, *Combustion Science and Technology, 190* (2018), 11, pp. 1886-1899.

[15] Kim, C. H., *et al.*, Soot Surface Growth and Oxidation in Laminar Diffusion Flames at Pressures of 0.1–1.0 Atm, *Combustion and flame, 136* (2004), 1-2, pp. 191-207.

[16] Hu, L. H., *et al.*, Axial Temperature Profile in Vertical Buoyant Turbulent Jet Fire in a Reduced Pressure Atmosphere, *Fuel, 106* (2013), Apr., pp. 779-786.

[17] Li, H. H., *et al.*, Effect of Pressure and Type of Fuel on Laminar Diffusion Flame Height at Subatmospheric Pressures, *Chemistry and Technology of Fuels and Oils, 51* (2015), 4, pp. 389-396.

[18] Zhang, X. C., *et al.*, Non-Dimensional Correlations on Flame Height and Axial Temperature Profile of a Buoyant Turbulent Line-Source Jet Fire Plume, *Journal of Fire Sciences, 32* (2014), 5, pp. 406-416.

[19] Wang, Q., *et al.*, Lift-off of Jet Diffusion Flame in Sub-atmospheric Pressures: An Experimental Investigation and Interpretation Based on Laminar Flame Speed, *Combustion and Flame, 161* (2014), 4, pp. 1125-1130.

[20] Wang, Q., *et al.*, Blow-out Limits of Nonpremixed Turbulent Jet Flames in a Cross Flow at Atmospheric and Sub-atmospheric Pressures. *Combustion and Flame, 162* (2015), 10, pp. 3562-3568.

[21] Wieser, D., *et al.*, The Influence of High Altitude on Fire Detector Test Fires, *Fire Safety Journal, 29* (1997), 2-3, pp. 195-204.

[22]Li, Z. H., *et al.*, Combustion Characteristics of n-Heptane and Wood Crib Fires at Different Altitudes, *Proceedings of the Combustion Institute, 32* (2009), 2, pp. 2481-2488.

[23] Hu, X. K., *et al.*, Combustion Characteristics of n-Heptane at High Altitudes, *Proceedings of the Combustion Institute, 33* (2011), 2, pp. 2607-2615.

[24] Hu, L. H., *et al.*, Pool Fire Flame Base Drag Behavior with Cross Flow in a Sub-Atmospheric Pressure, *Proceedings of the Combustion Institute, 36* (2017), 2, pp. 3105-3112.

[25] Liu, J. H., *et al.*, Experimental Study on Burning Behaviors of Liquid Fuels with Different Sooting Levels at High Altitude, *Thermal Science, 21* (2016), 6A, pp. 2533-2541.

[26] Jovanović, R. D., *et al.*, Experimental and Numerical Investigation of Flame Characteristics During Swirl Burner Operation under Conventional and Oxy-Fuel Conditions, *Thermal Science, 21* (2017), pp. 1463-1477.

[27] Zhang, N., *et al.*, On the Laminar Combustion Characteristics of Natural Gas-Syngas-Air Mixtures, *Thermal Science, 22* (2018), 5, pp. 2077-2086.

[28] Javareshkian, A., *et al.*, An Experimental Study on the Effects of Swirling Oxidizer Flow and Diameter of Fuel Nozzle on Behaviour and Light Emittance of Propane-Oxygen Non-Premixed Flame, *Thermal Science, 21* (2017), 3, pp. 1453-1462.

[29] Umyshev, D. R., *et al.*, Experimental Investigation of V-Gutter Flameholders, *Thermal Science, 21* (2017), 2, pp. 1011-1019.

[30] Zhang, X. L., *et al.*, Flame projection distance of horizontally oriented buoyant turbulent rectangular jet fires, *Combustion and Flame, 176* (2017), Feb., pp. 370-376.

[31]Tao, C., *et al.*, Experimental determination of flame length of buoyancy-controlled turbulent jet diffusion flames from inclined nozzles, *Applied Thermal Engineering, 93* (2016), pp. 884-887.